Dynamic Modeling of a Hydrogel-based Continuum Robotic Arm with Experimental Validation

Azadeh Doroudchi, Roozbeh Khodambashi†, Amir Salimi Lafmejani†,
Daniel M. Aukes, and Spring Berman

***Abstract*— Control of robots with soft actuators is still challenging due to the complexity of modeling actuator material dynamics in conjunction with the robot dynamics. In this paper, we introduce a 45-mm-long soft continuum robot with distributed local actuators in the form of cubes composed of a novel temperature-responsive hydrogel, each with an embedded Joule heater. We refer to these as *soft voxel actuators (SVAs)*. We present a dynamical model of this hydrogel-based continuum robot based on Cosserat rod theory. We experimentally identify the relationship between step input voltages applied to the SVAs and their resulting force outputs. In addition, we identify other unknown parameters of the model using vibration tests with the robot. We then numerically solve the Cosserat model and compare simulations of the model to measurements of the robot's tip displacement over time during open-loop control trials in which subsets of the SVAs are actuated. The normalized root-mean-square errors (NRMSEs) between the simulated and experimentally measured displacements are below 10%, which demonstrates the accuracy of the Cosserat model in describing the dynamics of the hydrogel-based continuum robot.**

NOMENCLATURE

$(\cdot)^*$	Value at the undeformed reference shape
$(\cdot)^h$	Time derivative's historical term
$(\cdot)_s$	Partial derivative with respect to arc length
$(\cdot)_t$	Partial derivative with respect to time
$\odot$	Element-wise multiplication
ρ	Material density (kg/m^3)
ρ_w	Water density (kg/m^3)
$\boldsymbol{B}_{bt}$	Damping matrix for bending and twisting (N$\cdot$m$^2\cdot$s)
$\boldsymbol{B}_{se}$	Damping matrix for shear and extension (N$\cdot$s)
$\boldsymbol{e}_3$	Unit vector $[0 \quad 0 \quad 1]^{\mathrm{T}}$
$\boldsymbol{f}$	Distributed force in the global frame (N/m)
$\boldsymbol{g}$	Gravitational acceleration vector (m/s^2)
$\boldsymbol{J}$	Second mass moment of inertia tensor (m^4)
$\boldsymbol{K}_{bt}$	Stiffness matrix for bending and twist (N$\cdot$m^2)
$\boldsymbol{K}_{se}$	Stiffness matrix for shear and extension (N)
$\boldsymbol{l}$	Distributed moment in the global frame (N$\cdot$m/m)
$\boldsymbol{m}$	Internal moment in the global frame (N$\cdot$m)
$\boldsymbol{n}$	Internal force in the global frame (N)
$\boldsymbol{p}$	Global position in Cartesian coordinates (m)
$\boldsymbol{q}$	Velocity in the local frame (m/s)
$\boldsymbol{R}$	Rotation matrix of backbone orientation
$\boldsymbol{r}$	Vector from SVA center of mass to the closest point on the backbone
$\boldsymbol{u}$	Curvature vector in the local frame (1/m)
$\boldsymbol{v}$	Rate of change of position with respect to arc length in the local frame
$\boldsymbol{w}$	Angular velocity in the local frame (1/s)
$\widehat{(\cdot)}$	Cross product matrix of a vector
A	Cross-sectional area (m^2)
C	Damping coefficient (kg/m^2)
c_0	Implicit difference coefficient for a state at t (1/s)
E	Young's modulus (Pa)
G	Shear modulus (Pa)

†These authors contributed equally to the paper.

This work was supported by Office of Naval Research (ONR) Award N00014-17-1-2117.

A. Doroudchi and A. Salimi Lafmejani are with the School of Electrical, Computer and Energy Engineering, Arizona State University (ASU), Tempe, AZ, 85287 {adoroudc,asalimil}@asu.edu. R. Khodambashi and D. Aukes are with the Polytechnic School, ASU, Mesa, AZ, 85212 {rkhodamb,danaukes}@asu.edu. S. Berman is with the School for Engineering of Matter, Transport and Energy, ASU, Tempe, AZ, 85287 {spring.berman}@asu.edu.

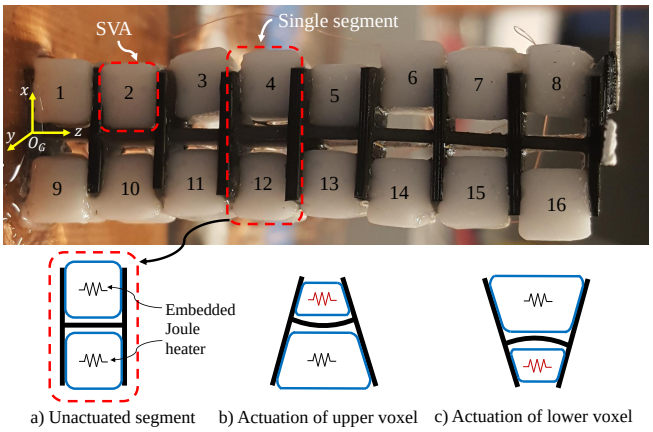

Fig. 1. *Top:* Soft continuum robot fabricated from a 3D-printed elastic material that supports 16 soft voxel actuators (SVAs) with embedded Joule heaters that actuate the robot. Each segment contains two SVAs. The global coordinate frame is shown in yellow. *Bottom:* Illustrations of a single segment in which: a) both SVAs are in the unactuated state; b) the upper SVA is actuated, causing the backbone to bend upward; c) the lower SVA is actuated, causing the backbone to bend downward.

I. INTRODUCTION

There is a diverse range of bio-inspired soft robots, many of which are designed to imitate human or animal capabilities. Robots composed of highly deformable matter such as fluids, gels, and elastomers [1], with soft actuators such as shape memory alloys (SMAs) and soft sensors such as artificial skin with touch and temperature receptors, comprise a new generation of robots that are capable of flexible movements and delicate interactions [2]. Such robots have extensive potential uses in healthcare applications, robotic exploration tasks, and cooperative human assistance.

A popular design for soft robots that provides capabilities beyond the scope of traditional rigid-link robots is a continuous rod-like curving manipulator. These soft robots which resemble biological trunks and tentacles are technically called continuum soft robots [3]. A general dynamical theory of rods, which undergo large deformations in space by bending, torsion, extension, and shear, can be employed for modeling continuum-like robots. This dynamical modeling approach is called the special Cosserat theory of rods [4]. There are examples of using Cosserat theory to model 1D elastic rods [5] and active cannulas [6] with torsion. Cosserat-based kinematic and dynamic approaches are included in the geometric mechanics of locomotion of bio-inspired robots modeled after animals with elongated bodies, such as snakes, worms, and caterpillars [7], or octopus arms [8], [9]. The Cosserat theory has also been widely used in studies of different actuation systems, such as pneumatic muscle-actuated multi-section prototype continuum arms [10], fluidic-actuated legs of the soft crawler FASTT presented in [11], and tendon-driven robots [12]. The work [13] presents a numerical approach for real-time simulation of the forward dynamics of Cosserat-based robot models. In this approach, the time derivatives of the Cosserat partial differential equations (PDEs) of motion are implicitly discretized, and then the resulting ODE boundary value problem (BVP) in arc length is solved at each time step. It is shown that the approach is suitable for a wide range of robot models and numerical schemes. In this paper, we apply the Cosserat model and simulation methodology developed in [13] to characterize the dynamics of a hydrogel-based continuum robot.

Smart hydrogels are new materials whose properties make them excellent candidates for soft robotic and biomedical applications [14]. A hydrogel is composed of a hydrophilic multiphase polymer mixture that may exhibit properties of both solids and liquids. Its structural framework is formed from 3D networks of randomly cross-linked polymeric chains that embody three different phases: solid polymer network matrix, interstitial water or biological fluid, and ion species [15]. Hydrogels require water to function and can be used as deformable actuators that are lightweight and noiseless, in contrast to pneumatic and hydraulic actuators. There are various types of hydrogels that deform when they are stimulated with different sources of energy [16], [17]. Poly(N-isopropylacrylamide), or PNIPAAM, is a temperature-responsive hydrogel that contracts when heated by a laser, electrical resistor, hot water, or other source [18]. Nano-structured smart hydrogels exhibit rapid stimuli-responsive characteristics, as well as highly elastic properties that enable them to sustain large compression forces, resist slicing, and withstand deformations such as bending, twisting, and extensive stretching [19]. Despite extensive research on macroscale robots and microelectromechanical systems, relatively little attention has been paid to the development of miniature soft robots with diverse shapes, actuation mechanisms, and integrated functionalities. Some existing hydrogel-based robots are described in [20], which presents micro- to millimeter-scale soft aquabots that perform multi-functional operations, and [21], which presents a 3D-printed electro-responsive bending actuator for biomedical applications.

We have designed and fabricated a novel soft continuum robot using temperature-responsive hydrogel material with embedded-Joule heaters that produce bending motions when they are actuated. The robotic arm is constructed from a 3D-printed elastic backbone with orthogonal plates glued to sixteen SVAs which can be actuated independently to create local deformations, as shown in Fig. 1. A force measurement experiment was conducted in order to identify the relationship between the Joule heater input voltage and the SVA output force applied to the interacting surface during contraction and expansion. In order to estimate the unknown mechanical parameters of the robot, we conducted vibration tests in which we measured Young's modulus and the damping coefficient of the robot, under the assumption that the robot could be approximated as a homogeneous material. We numerically solved the Cosserat model using the shooting method and compared it to experimental measurements of the robot tip's vertical deflection under open-loop control, during which different groups of SVAs were actuated and caused the robot to bend in a single plane.

Section II describes the fabrication details of the hydrogel-based continuum robot. The Cosserat dynamic model of the soft continuum robot is derived in Section III. The procedure for the hydrogel actuator identification is presented in Section IV. Simulation, calibration, and model verification results are discussed in Section V.

II. Robot Design and Fabrication

As illustrated in Fig. 1, the soft continuum robot is a cantilevered arm fabricated from a 3D-printed elastic backbone with orthogonal plates that support 16 cubical soft voxel actuators (SVAs), which are composed of a smart hydrogel material. Each SVA contracts when it is heated by its embedded Joule heater, and when the heater is turned off, it swells back to its initial shape. The SVA's actuation causes the backbone to bend at the corresponding *segment* (outlined in Fig. 1), and as a result, the robot's tip exhibits a deflection along the x-axis. Multiple SVAs can be configured as elastic beams or rods with different numbers of degrees of freedom (DoF). Our ultimate goal is to construct an SVA-acuated robot that can deform in 3D and imitate the four motions of elongation, shortening, bending, and twisting that occur in an octopus arm [22]. Our current soft continuum robot has 16 actuators that can produce bending motions in the $x-z$ plane in Fig. 1.

In order to fabricate the SVAs, we used standard PNIPAAM hydrogel precursor solution, along with a proprietary recipe described in [23] which was poured into molds using pipettes while the resistive heater ($10\,\Omega$ SMD resistor 0805) was held in place using grippers. A UV LED (UV 365nm, 10W, Shenzhen Chanzon Technology Co., Ltd., China) was used for curing the gels. After curing, the actuator was placed in a vessel containing deionized (DI) water. The water was changed several times every few hours in order

to wash away the solvents. Once fully swollen, each SVA has the dimensions 4.5×4.5×4.5 mm and weighs 0.125 g. To create the hydrogel-based continuum robot, a 4.5×11×45 mm elastic backbone with orthogonal plates was 3D-printed, and the SVAs were affixed to the plates using superglue. When all 16 SVAs are fully swollen, the total mass of the robot is 3 g, and its density (ρ) is 1346.8 $\mathrm{kg/m^3}$.

Each SVA can be selectively commanded as a local actuator. To actuate an SVA, an input voltage is sent to 0.08 mm-diameter copper wires that protrude from the SVA's embedded-Joule heater and are connected to the electrical circuit boards. An Arduino Mega 2560 acts as a communication hub between MATLAB and a MOSFET board (PCA9685 National Control Devices, Osceola, Missouri, U.S.A.). This board has 16 channels, each of which activates one of the 16 actuators of the continuum robot (16 output PWM channels that can produce up to 8 watts of power per channel). The MOSFET board receives the values of the PWM ratio and the channel number and then activates the corresponding Joule heater.

III. Dynamic Modeling

We use Cosserat rod theory to model the nonlinear dynamics of the hyperelastic hydrogel-based continuum robot. Since this model accounts for the effect of bending, torsion, shear, and extension, it can accurately describe all the motions of the soft continuum robot. Although our current robot can only exhibit bending motions, Cosserat rod theory provides a more accurate dynamic model than the Kirchhoff and Euler-Bernoulli models [24]. While the Kirchhoff model is also nonlinear, it only incorporates the effects of shear and extension, and the Euler-Bernoulli model, which is linear, cannot be used to describe large deformations. In our previous work [25], we used the Euler-Bernoulli model for decentralized vibration control of a segmented soft continuum robot in simulation, but specified that the robot's length-to-diameter ratio was large enough to satisfy the small-deformation condition.

We use the method presented in [13] to develop a dynamic model of our robot. In this method, the Cosserat PDEs are converted into a reduced system of ODEs by substituting semi-discretized distributed force and rotational inertia terms into the original PDEs. Here, *semi-discretized* indicates that the terms are discretized with respect to space, but not time. We note that the notation in our model is defined in the Nomenclature section of this paper. In [13], the general Cosserat PDEs are reduced to the following system of ODEs in arc length s:

$$\begin{aligned}
\boldsymbol{p}_s &= \boldsymbol{R}\boldsymbol{v} \\
\boldsymbol{R}_s &= \boldsymbol{R}\widehat{\boldsymbol{u}} \\
\boldsymbol{n}_s &= \rho A\boldsymbol{R}(\widehat{\boldsymbol{w}}\boldsymbol{q} + \boldsymbol{q}_t) - \boldsymbol{f} \\
\boldsymbol{m}_s &= \rho\boldsymbol{R}(\widehat{\boldsymbol{w}}\boldsymbol{J}\boldsymbol{w} + \boldsymbol{J}\boldsymbol{w}_t) - \widehat{\boldsymbol{p}}_s\boldsymbol{n} - \boldsymbol{l} \\
\boldsymbol{q}_s &= \boldsymbol{v}_t - \widehat{\boldsymbol{u}}\boldsymbol{q} + \widehat{\boldsymbol{w}}\boldsymbol{v} \\
\boldsymbol{w}_s &= \boldsymbol{u}_t - \widehat{\boldsymbol{u}}\boldsymbol{w}
\end{aligned} \tag{1}$$

In these equations, the position, orientation, internal force and moment, and linear and angular velocities of the elastic backbone are calculated for every segment. In the numerical solution of these equations, the rate of change of position $\boldsymbol{v}$, curvature vector $\boldsymbol{u}$, linear velocity $\boldsymbol{q}$, angular velocity $\boldsymbol{w}$, and their time derivatives are algebraically calculated from variables at the current and previous time steps using the shooting method. As explained in more detail in [13], the semi-discretization method is used to approximate the time derivatives of these state variables in terms of the values of the variables with coefficient c_0 at the current time step and functions of the history of the variables, as follows:

$$\begin{aligned}
\boldsymbol{v}_t &= c_0\boldsymbol{v} + \boldsymbol{v}^h \\
\boldsymbol{u}_t &= c_0\boldsymbol{u} + \boldsymbol{u}^h \\
\boldsymbol{q}_t &= c_0\boldsymbol{q} + \boldsymbol{q}^h \\
\boldsymbol{w}_t &= c_0\boldsymbol{w} + \boldsymbol{w}^h
\end{aligned} \tag{2}$$

The variables $\boldsymbol{v}$ and $\boldsymbol{u}$ are computed as:

$$\begin{aligned}
\boldsymbol{v} &= (\boldsymbol{K}_{se} + c_0\boldsymbol{B}_{se})^{-1}(\boldsymbol{R}^T\boldsymbol{n} + \boldsymbol{K}_{se}\boldsymbol{v}^* - \boldsymbol{B}_{se}\boldsymbol{v}^h), \\
\boldsymbol{u} &= (\boldsymbol{K}_{bt} + c_0\boldsymbol{B}_{bt})^{-1}(\boldsymbol{R}^T\boldsymbol{m} + \boldsymbol{K}_{bt}\boldsymbol{u}^* - \boldsymbol{B}_{bt}\boldsymbol{u}^h),
\end{aligned} \tag{3}$$

where the effects of shear and extension are characterized by $\boldsymbol{K}_{se}$ and the effects of bending and torsion by $\boldsymbol{K}_{bt}$, under the assumption that the robotic arm is homogeneous, isotropic, and symmetric:

$$\boldsymbol{K}_{se} = \begin{bmatrix} G & 0 & 0 \\ 0 & G & 0 \\ 0 & 0 & E \end{bmatrix} A, \quad \boldsymbol{K}_{bt} = \begin{bmatrix} E & 0 & 0 \\ 0 & E & 0 \\ 0 & 0 & G \end{bmatrix} \boldsymbol{J}. \tag{4}$$

In Eq. (3), $\boldsymbol{B}_{se} = \tau\boldsymbol{K}_{se}$ and $\boldsymbol{B}_{bt} = \tau\boldsymbol{K}_{bt}$, where τ is twice the period of the vibrations exhibited by the robot's tip during the tests described in Section V.

Similar to the simulated fluidic soft robot considered in Section 5.3 of [13], which is subject to distributed forces and moments, our robot experiences distributed forces and moments on its backbone, in part produced by the SVAs when they are actuated individually. The external forces and moments on the backbone are denoted by $\boldsymbol{f}$ and $\boldsymbol{l}$, respectively, and are defined as follows:

$$\begin{aligned}
\boldsymbol{f} &= (\rho - \rho_w)A\boldsymbol{g} - \boldsymbol{R}\boldsymbol{C}\boldsymbol{q} \odot |\boldsymbol{q}| + \boldsymbol{f}_{seg} + \boldsymbol{f}_{ext}\ , \\
\boldsymbol{l} &= \boldsymbol{l}_{seg} + \boldsymbol{l}_{ext}\ .
\end{aligned} \tag{5}$$

The first two terms in the equation for $\boldsymbol{f}$ describe the robot's weight in water and the drag force, respectively. The matrix $\boldsymbol{C} = \boldsymbol{I} * C$ is calculated from the vibration tests discussed in Section V. The force and moment applied by each SVA to the backbone of its corresponding segment are denoted by $\boldsymbol{f}_{seg}$ and $\boldsymbol{l}_{seg}$, respectively. The external force and moment on this part of the backbone due to environmental disturbances are denoted by $\boldsymbol{f}_{ext}$ and $\boldsymbol{l}_{ext}$, respectively. We can write $\boldsymbol{f}_{seg}$ and $\boldsymbol{l}_{seg}$, which are expressed in the global frame (O_G), in terms of f_a, the magnitude of an SVA's force in the local frame:

$$\begin{aligned}
\boldsymbol{f}_{seg} &= f_a\boldsymbol{R}_s\boldsymbol{e}_3, \\
\boldsymbol{l}_{seg} &= f_a\boldsymbol{R}[(\boldsymbol{v} + \widehat{\boldsymbol{u}}\boldsymbol{r}) \times \boldsymbol{e}_3 + \boldsymbol{r} \times \widehat{\boldsymbol{u}}\boldsymbol{e}_3].
\end{aligned} \tag{6}$$

As can be seen from the illustrations in Fig. 1, f_a is zero when both SVAs in a segment are unactuated, and it is non-zero when one SVA is actuated. Note that since the robot cannot undergo elongation or shortening in the axial direction, both SVAs of a segment cannot be actuated simultaneously. The dependence of the direction of $\boldsymbol{l}_{seg}$ on the direction of the vector $\boldsymbol{r}$ is determined by the particular SVA that is actuated in the corresponding segment. In order to numerically solve the above set of equations (6) for each segment, the value of f_a is required. In the next section, we identify the relationship between the voltage input to an SVA and its applied force on the plate that supports it.

IV. Actuator Identification

The free energy of the hydrogel results from two molecular processes: stretching the hydrogel network and mixing the network with the small hydrogel molecules [26]. The hydrogel can undergo large deformation in two modes: a fast process with only shape change, and a slow process with both shape and volume changes. In [27], the chemical potential of the solvent and the deformation gradient of the network are defined as the independent variables of the free-energy function, and it is shown that the boundary value problem of the swollen gel is equivalent to that of a hyperelastic solid. To implement their approach, finite-element packages such as ABAQUS or COMSOL are required to analyze the hydrogel dynamics [28]. These software packages cannot solve the hydrogel dynamic problem in real-time simultaneously with the control program when the robot is actuated, even when using LiveLink™ for MATLAB.

In order to solve the hydrogel dynamic equations in real-time, we need to either measure the force magnitude f_a in real-time or estimate it from the input voltage. Toward this end, we have designed an experimental setup in order to find the relationship between the input voltage and output force of an SVA. As shown in Fig. 2, we measure the tensile force applied by an SVA when it is actuated while bounded by two plates, similar to its configuration on the robot. In this setup, one side of an SVA is glued to a fixed plate at the bottom of a water chamber, and the other side is glued to a force sensor (load cell). The copper wires of the Joule heater are connected to grippers, which are connected to the control board in order to receive an input voltage signal. The data from the force sensor is sent to the computer using a PhidgetBridge 1046_0B bridge interface and a Micro Load Cell (0-100 g) - CZL639HD module.

From the properties of the hydrogel, we know that shape and volume changes occur in the operating region between 25°C and 32°C. Considering the resistance of the Joule heater, the range of voltages that we can use to actuate the SVA in order to stay within this operating region is 0 V to 3.7 V. We recorded measurements of the SVA output force over time within this voltage range, at a resolution of 0.18 V, for step input voltages with amplitude V. Since each SVA is affixed to plates that are orthogonal to the backbone of the robot, the SVA applies a tensile force of f_a to these plates when actuated. We applied the voltage for a length of time

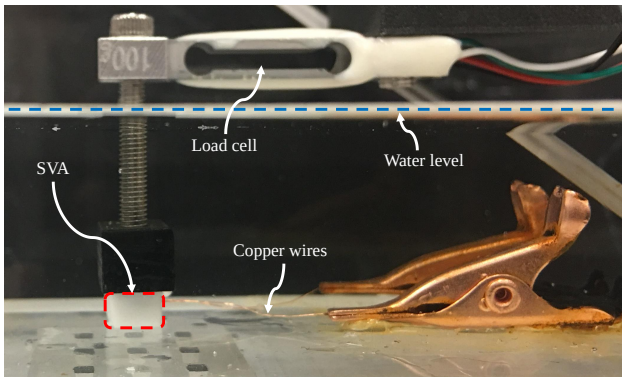

Fig. 2. Experimental setup that uses a load cell to measure the force applied by an SVA.

TABLE I
Values of coefficients in Eq. (8).

Coefficient	Value	Coefficient	Value	Coefficient	Value
d_{11}	0.0024	d_{21}	0.4900	d_{31}	0.0383
d_{12}	-0.0004	d_{22}	0.1564	d_{32}	0.0002

which ensured that the SVA had fully contracted, and was therefore exerting its maximum possible force.

Figure 3 illustrates the measured tensile force produced by the SVA over time when it was actuated with different step input voltage amplitudes for 40 seconds. During the first 40 seconds, the applied voltage heated the SVA, and thereafter the voltage was set to zero and the SA cooled down as a result of convective heat transfer to the surrounding water, which was kept at a constant temperature of 25°C. As the figure shows, the SVA force output f_a over time t and the input voltage amplitude V have a proportional relationship: higher forces are produced when higher voltages are applied. We determined an equation for f_a in terms of t and V, for the 20 values of V that we used in our tests, by applying black-box identification techniques for input-output data [29]:

$$f_a(V,t) = \frac{b_0}{b_2}\left(1 + \mathrm{e}^{-\frac{b_1 t}{2}}\left(\cosh\left(\sqrt{\frac{{b_1}^2}{4} - b_2}\, t\right) + \frac{b_1 \sinh\left(\sqrt{\frac{{b_1}^2}{4} - b_2}\, t\right)}{2\sqrt{\frac{{b_1}^2}{4} - b_2}}\right)\right), \quad 0 \le V \le 3.7,\ t \ge 0. \tag{7}$$

We identified the b_i coefficients as the following functions of V using the System Identification and Curve Fitting Toolboxes in MATLAB:

$$\begin{aligned} b_0 &= d_{11}V + d_{12}, \\ b_1 &= d_{21}V^2 + d_{22}, \\ b_2 &= d_{31}V + d_{32}. \end{aligned} \tag{8}$$

The values of the identified coefficients d_{ij} are listed in Table I.

Figure 4 compares the measured force over time to the identified function for $f_a(V,t)$ in Eq. (7) for the case where

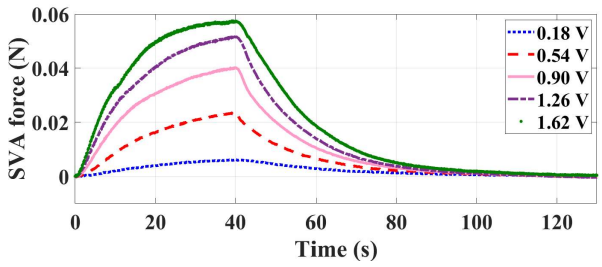

Fig. 3. Measured force applied by an SVA while it is actuated by different step input voltages for 40 s.

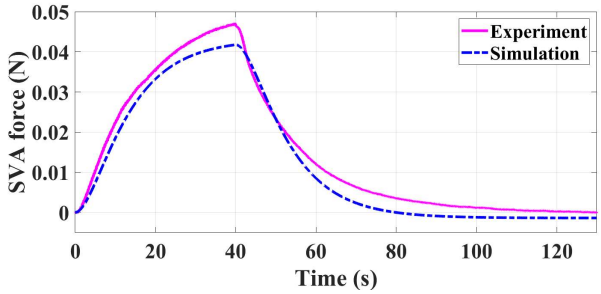

Fig. 4. Simulation of the identified force function (7) compared to the experimentally measured force for the case of an SVA actuated by a 1.08 V step input for 40 s.

an SVA is actuated with a 1.08 V step input for 40 seconds. The resulting root-mean-square error (RMSE) between the two plots is 0.0026 N. To compare the RMSE values for the different input voltages, we calculated the normalized root-mean-square error (NRMSE) for each voltage. This error was relatively low, under 5%, for all input voltage amplitudes that were tested. We leave model validation for more complicated input voltages for future work on closed-loop control of the robot.

V. Experimental Validation and Discussion

In this section, we validate the Cosserat dynamical model from Section III by comparing simulations of the model to experimental data for open-loop actuation of the robot. Some parameters of the model are estimated experimentally using vibration tests.

A. Vibration tests

The Young's modulus and physical damping coefficient of the robot are not readily available, since the robot is in reality neither homogeneous nor isotropic. Moreover, the submergence of the robot in water during the experiments affects the damping coefficient. In order to estimate the unknown parameters in the dynamical model, we make the approximation that the robot is homogeneous and isotropic. We perform the widely-used weight (or force) experiment [30] with different values of weights to produce vibrations of the robot's tip until it reaches its equilibrium position. The vibration tests are performed on the robot with the SVAs in their fully swollen state. Figure 5 shows side and front views of the robot bending when a 0.405 g load is placed on its tip

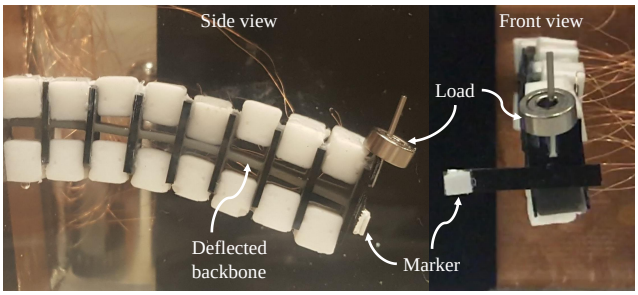

Fig. 5. Side and front views of the continuum robot during a vibration test in which a 0.405 g load is placed on its tip.

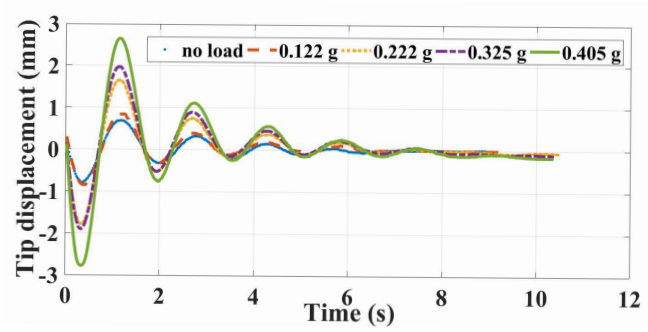

Fig. 6. Vibrations of the robot's tip around its equilibrium position (shifted to 0 mm) for cases with no weight attached and with attached weights of 0.122 g, 0.222 g, 0.325 g, and 0.405 g. The period of the vibrations is 1.56 s.

during a vibration test. A Logitech C930e webcam placed in front of the chamber is used to track the white square marker on the robot's tip, labeled in Fig. 5, in order to measure the tip's position over time.

Figure 6 plots the robot's vibrations around equilibrium in five cases. In case 1, it is deflected upward and then released to vibrate freely, and in cases 2 through 5, a load of 0.122 g, 0.222 g, 0.325 g, and 0.405 g, respectively, is rapidly added to its tip. To clearly compare the time responses of the robot's deflection, its equilibrium position along the x-axis (see Fig. 1) for each case is shifted to 0 mm. The actual equilibrium positions for cases 1 to 5 were -0.29, -4.25, -4.71, -7.39, and -7.89 mm, respectively.

We measured the amplitudes of the vibrations at adjacent peaks for different cases, and determined the damping ratio from the logarithmic decrements of these measurements [31]. Using the structural damping equations for cantilevered beams and spring-mass systems, the damping coefficient and Young's modulus values were calculated as $0.0262\,\mathrm{kg/m^2}$ and 2.005 kPa, respectively.

B. Verification of the dynamical model

Having estimated the unknown parameters and measured the SVA applied tensile forces, we were able to simulate the robot forward dynamics in MATLAB using Eqs. (1)–(8). Every segment's position and orientation were calculated at each iteration of the simulation. We tested eight cases in both simulation and experiment, in which the robot was actuated in an open-loop manner with square signals of voltage that

TABLE II

ERRORS BETWEEN MEASURED AND SIMULATED ROBOT TIP DISPLACEMENTS.

Case number	Actuators number	Voltage (V)	RMSE (mm)	$\lvert\overline{X}\rvert$ (mm)	NRMSE (%)
1	1-8	1.8	0.28	4.09	6.8%
2	1-8	3.6	0.69	8.96	7.7%
3	9-16	1.8	0.39	6.51	5.9%
4	9-16	3.6	0.63	13.06	4.8%
5	3,4,5	3.6	0.36	4.98	7.2%
6	14,15,16	3.6	0.16	2.01	7.9%
7	7,8,11,12,13	3.6	0.49	5.15	9.5%
8	4,9,15	3.6	0.32	3.52	9.1%

were applied to different subsets of SVAs. Table II lists the parameters for our eight test cases, including the numbers of the particular SVAs that are actuated with their corresponding input voltages, which were all applied for 15 seconds. The RMSE values in the table give the errors between the robot's tip position in experiment and simulation during one test for each case, and $\overline{X} = X_{max} - X_{min}$ indicates the tip's maximum displacement from its initial position. Dividing RMSE by $|\overline{X}|$ yields the NRMSE value, for which the percentages are reported. These relatively low NRMSE values, which are all under 10%, indicate the accuracy of the modeling approach. Figures 7(a) and 7(b) show the simulated and experimental deformations of the robot for Case 4, where SVAs number 9 to 16 were actuated by 3.6 V for 15 s.

Figure 8(a) plots the simulated and experimentally measured displacement of the robot's tip for the case when all SVAs in the top row (numbered 1 to 8) are actuated with a square wave of amplitude 1.8 V for 60 seconds and then 0 V for 60 seconds. The RMSE between the plots is 0.68 mm. Figure 8(b) plots the simulated and measured displacements for the case when SVA numbers 4, 9, and 15 are actuated with a square wave of amplitude 3.6 V for 15 seconds. The RMSE between the plots for this case is 0.32 mm. Since the delay in the hydrogel response is not included in the SVA force model or the robot dynamical model, at the beginning of the SVA heating state or cooling state and in general during any change of states, error arises between the simulations and experimental measurements, as is apparent from the results in Fig. 8. Other sources of error between the simulations and experiments include deviations from the assumption of a homogeneous and isotropic robot, inconsistencies in SVA fabrication (which can be addressed in future work), and variable hydrogel stiffness during the contraction and swelling modes.

VI. CONCLUSION

In this paper, a new hydrogel-actuated continuum robotic arm is presented, and its dynamics are modeled based on the Cosserat theory of rods. The robot is designed to bend when one or more of the actuators located along its length, called SVAs, are actuated by embedded Joule heaters. To measure the force applied by the SVAs during actuation, an experimental setup was designed to obtain input-output data on the voltage-to-force relationship, which was characterized using black-box identification techniques. Experimental validation results demonstrate that the identified model has an NRMSE of at most 5% over a range of step input voltages (0 V–3.7 V). The dynamic model was also validated in MATLAB simulations after estimating unknown mechanical parameters of the robot in an experimental vibration test. By comparing the physical robot's deformation under open-loop control with predefined actuation patterns to the corresponding simulation results, we show that the model accurately reproduces the robot dynamics, with at most 10% NRMSE. In future work, we will incorporate shear and torsion effects into our models for new designs of hydrogel-based continuum robots that can deform in 3D. Moreover, we will develop decentralized controllers for such robots, with the goal of performing more complex tasks such as position control of the tip, trajectory tracking, shape control, and object manipulation.

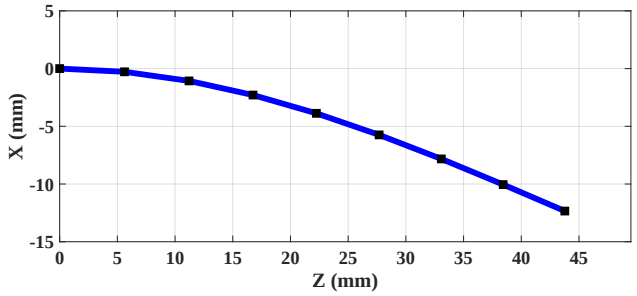

(a)

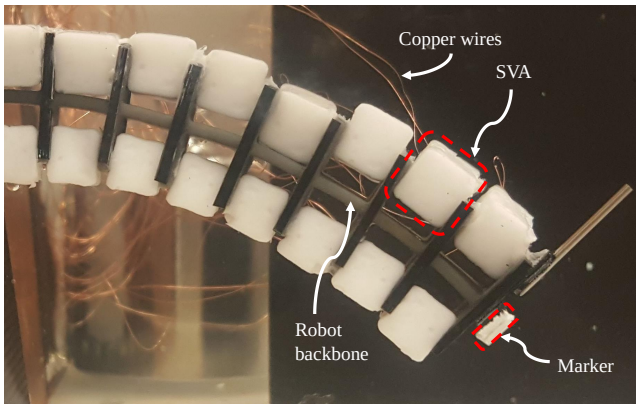

(b)

Fig. 7. Continuum robot bending when its bottom row of SVAs (numbers 9 to 16) have been actuated by a square wave with amplitude 3.6 V applied for 15 seconds (Case 4, Table II): (a) simulation; (b) experiment.

REFERENCES

[1] C. Majidi, "Soft robotics: a perspective—current trends and prospects for the future," *Soft Robotics*, vol. 1, no. 1, pp. 5–11, 2014.

[2] R. Pfeifer, M. Lungarella, and F. Iida, "The challenges ahead for bio-inspired'soft'robotics," *Communications of the ACM*, vol. 55, no. 11, pp. 76–87, 2012.

[3] D. Rus and M. T. Tolley, "Design, fabrication and control of soft robots," *Nature*, vol. 521, no. 7553, pp. 467–475, 2015.

[4] S. S. Antman, "Nonlinear plasticity," in *Nonlinear Problems of Elasticity*. Springer, 1995, pp. 603–628.

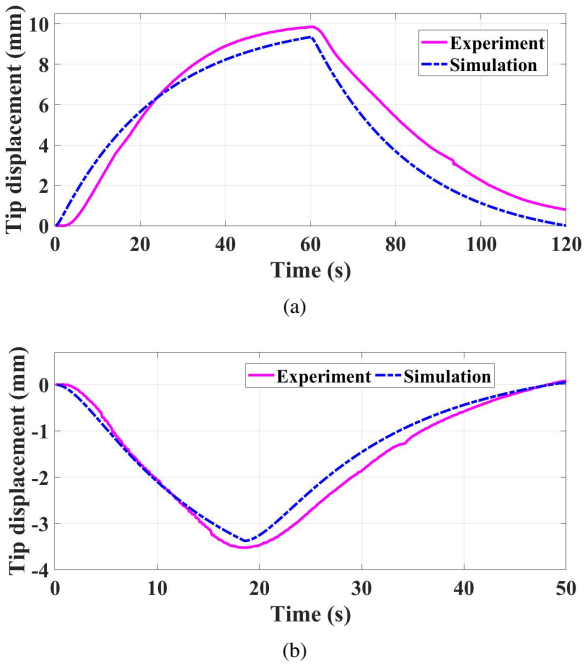

Fig. 8. Simulated and measured robot tip displacement along the x-axis when (a) SVA numbers 1 to 8 are actuated with a square wave of amplitude 1.8 V applied for 60 seconds; (b) SVA numbers 4, 9, and 15 are actuated with a square wave of amplitude 3.6 V for 15 seconds (Case 8, Table II).

[5] J. Spillmann and M. Teschner, "CoRdE: Cosserat rod elements for the dynamic simulation of one-dimensional elastic objects," in *Proceedings of the 2007 ACM SIGGRAPH/Eurographics symposium on Computer animation*. Eurographics Association, 2007, pp. 63–72.

[6] R. J. Webster III, J. M. Romano, and N. J. Cowan, "Mechanics of precurved-tube continuum robots," *IEEE Transactions on Robotics*, vol. 25, no. 1, pp. 67–78, 2008.

[7] F. Boyer, S. Ali, and M. Porez, "Macrocontinuous dynamics for hyperredundant robots: application to kinematic locomotion bioinspired by elongated body animals," *IEEE Transactions on Robotics*, vol. 28, no. 2, pp. 303–317, 2011.

[8] D. Trivedi, A. Lotfi, and C. D. Rahn, "Geometrically exact models for soft robotic manipulators," *IEEE Transactions on Robotics*, vol. 24, no. 4, pp. 773–780, 2008.

[9] C. Laschi, B. Mazzolai, V. Mattoli, M. Cianchetti, and P. Dario, "Design of a biomimetic robotic octopus arm," *Bioinspiration & biomimetics*, vol. 4, no. 1, p. 015006, 2009.

[10] I. S. Godage, G. A. Medrano-Cerda, D. T. Branson, E. Guglielmino, and D. G. Caldwell, "Dynamics for variable length multisection continuum arms," *The International Journal of Robotics Research*, vol. 35, no. 6, pp. 695–722, 2016.

[11] F. Renda, V. Cacucciolo, J. Dias, and L. Seneviratne, "Discrete cosserat approach for soft robot dynamics: A new piece-wise constant strain model with torsion and shears," in *2016 IEEE/RSJ International Conference on Intelligent Robots and Systems (IROS)*. IEEE, 2016, pp. 5495–5502.

[12] F. Renda and C. Laschi, "A general mechanical model for tendon-driven continuum manipulators," in *2012 IEEE International Conference on Robotics and Automation*. IEEE, 2012, pp. 3813–3818.

[13] J. Till, V. Aloi, and C. Rucker, "Real-time dynamics of soft and continuum robots based on Cosserat rod models," *The International Journal of Robotics Research*, vol. 38, no. 6, pp. 723–746, 2019.

[14] A. Guiseppi-Elie, "Electroconductive hydrogels: synthesis, characterization and biomedical applications," *Biomaterials*, vol. 31, no. 10, pp. 2701–2716, 2010.

[15] H. Li, "Smart hydrogel modelling," *Springer*, 2009.

[16] X. Peng, C. Jiao, Y. Zhao, N. Chen, Y. Wu, T. Liu, and H. Wang, "Thermoresponsive deformable actuators prepared by local electrochemical reduction of poly (n-isopropylacrylamide)/graphene oxide hydrogels," *ACS Applied Nano Materials*, vol. 1, no. 4, pp. 1522–1530, 2018.

[17] M. Qin, M. Sun, M. Hua, and X. He, "Bioinspired structural color sensors based on responsive soft materials," *Current Opinion in Solid State and Materials Science*, vol. 23, no. 1, pp. 13–27, 2019.

[18] H. G. Schild, "Poly (N-isopropylacrylamide): experiment, theory and application," *Progress in polymer science*, vol. 17, no. 2, pp. 163–249, 1992.

[19] L.-W. Xia, R. Xie, X.-J. Ju, W. Wang, Q. Chen, and L.-Y. Chu, "Nano-structured smart hydrogels with rapid response and high elasticity," *Nature communications*, vol. 4, p. 2226, 2013.

[20] G. H. Kwon, J. Y. Park, J. Y. Kim, M. L. Frisk, D. J. Beebe, and S.-H. Lee, "Biomimetic soft multifunctional miniature aquabots," *Small*, vol. 4, no. 12, pp. 2148–2153, 2008.

[21] A. Zolfagharian, A. Z. Kouzani, S. Y. Khoo, A. Noshadi, and A. Kaynak, "3D printed soft parallel actuator," *Smart Materials and Structures*, vol. 27, no. 4, p. 45019, 2018. [Online]. Available: http://dx.doi.org/10.1088/1361-665X/aaab29

[22] W. M. Kier, "The musculature of coleoid cephalopod arms and tentacles," *Frontiers in cell and developmental biology*, vol. 4, p. 10, 2016.

[23] R. Khodambashi, Y. Alsaid, D. Aukes, and X. He, "Shape Morphing Soft Material," 2019, uS Provisional Patent 62/860,700.

[24] O. M. O'Reilly, *Modeling nonlinear problems in the mechanics of strings and rods*. Springer, 2017.

[25] A. Doroudchi, S. Shivakumar, R. E. Fisher, H. Marvi, D. Aukes, X. He, S. Berman, and M. M. Peet, "Decentralized control of distributed actuation in a segmented soft robot arm," in *2018 IEEE Conference on Decision and Control (CDC)*. IEEE, 2018, pp. 7002–7009.

[26] W. Hong, X. Zhao, J. Zhou, and Z. Suo, "A theory of coupled diffusion and large deformation in polymeric gels," *Journal of the Mechanics and Physics of Solids*, vol. 56, no. 5, pp. 1779–1793, 2008.

[27] W. Hong, Z. Liu, and Z. Suo, "Inhomogeneous swelling of a gel in equilibrium with a solvent and mechanical load," *International Journal of Solids and Structures*, vol. 46, no. 17, pp. 3282–3289, 2009.

[28] X. Wang, Z. Zhai, Y. Chen, and H. Jiang, "A facile, robust and versatile finite element implementation to study the time-dependent behaviors of responsive gels," *Extreme Mechanics Letters*, vol. 22, pp. 89–97, 2018.

[29] L. Ljung, "Black-box models from input-output measurements," in *IMTC 2001. Proceedings of the 18th IEEE instrumentation and measurement technology conference. Rediscovering measurement in the age of informatics (Cat. No. 01CH 37188)*, vol. 1. IEEE, 2001, pp. 138–146.

[30] J. Linn, H. Lang, and A. Tuganov, "Geometrically exact cosserat rods with kelvin–voigt type viscous damping," *Mechanical Sciences*, vol. 4, no. 1, pp. 79–96, 2013.

[31] H. Lang, J. Linn, and M. Arnold, "Multi-body dynamics simulation of geometrically exact cosserat rods," *Multibody System Dynamics*, vol. 25, no. 3, pp. 285–312, 2011.